


Changes in myelinated fibres in the hippocampus of streptozotocin-induced diabetic rats: a stereological investigation

Hui Zhao^{1*}, Ting Zhang^{2*}, Feng Zhao², Min Tan², Shijuan Du⁴, Yunzi Wang⁴, Juan Li⁴, Jiang Du⁵, Yong Tang⁶, Yuanyu Zhao³

¹Institute of Basic Medicine and Forensic Medicine, North Sichuan Medical College, Nanchong, Sichuan Province, China

²Laboratory of Electron Microscopy, North Sichuan Medical College, Nanchong, Sichuan Province, China

³Department of Pathology, Chengdu First People's Hospital, Chengdu, Sichuan Province, China

⁴Department of Pathology, Sichuan Science City Hospital, Mianyang, Sichuan Province, China

⁵Department of General Surgery, Sichuan Science City Hospital, Mianyang, Sichuan Province, China

⁶Department of Histology and Embryology, Chongqing Medical University, Chongqing, China

[Received: 5 March 2023; Accepted: 29 May 2023; Early publication date: 5 June 2023]

Diabetes causes cognitive impairment, and the hippocampus is important for long-term and permanent memory function. However, the mechanism of their interaction is still unclear. In this study, rat models of diabetes mellitus were generated by a single injection of streptozotocin (STZ). This study aims to explore the changes in myelinated fibres in the hippocampus of type 1 diabetic rats. The unbiased stereological methods and transmission electron microscopy were used to obtain the total volume of the hippocampus, the total volume of the myelin sheath, the total length of the myelinated nerve fibres, the distribution of the length with different diameters of the myelinated fibres, and the distribution of the length with different thickness of the myelin sheath. Stereological analysis revealed that, compared to that of the control group, the total myelinated fibres volumes and the total myelinated fibres length were decreased slightly, while the total volume and the thickness of myelin sheaths were significantly decreased in the diabetic group. Finally, when compared with the control group, the total length of myelinated fibres in the diabetes group was significantly reduced, with diameters ranging from 0.7 to 1.1 μm and thicknesses of myelin sheaths from 0.15 to 0.17 μm . This study provides the first experimental evidence by stereological means to demonstrate that myelinated nerve fibres may be the key factor in cognitive dysfunction in diabetes. (Folia Morphol 2024; 83, 2: 325–332)

Keywords: unbiased stereology, diabetes, hippocampus, myelinated fibre, transmission electron microscopy

INTRODUCTION

Diabetes is a chronic disease that can result in various systemic complications, affecting peripheral

tissues and the central nervous system. The most common diabetic brain complications include cognitive decline and depression [4, 19]. Diabetes-related

Address for correspondence: Yuanyu Zhao, Department of Pathology, Chengdu First People's Hospital, Chengdu, Sichuan Province, China; e-mail: yzhaoy2023@163.com

*Hui Zhao and Ting Zhang contributed equally to this work and share first authorship.

This article is available in open access under Creative Commons Attribution-Non-Commercial-No Derivatives 4.0 International (CC BY-NC-ND 4.0) license, allowing to download articles and share them with others as long as they credit the authors and the publisher, but without permission to change them in any way or use them commercially.

cognitive impairment is an increasingly recognized complication of type 1 diabetes (T1D). In recent years, it has been found that the central nervous system attains various functional disorders such as electrophysiological issues, cognitive disorders, and structural changes to the hippocampus which are imperative for learning and memory [15]. Loss of hippocampal neuroplasticity impairs the ability of the brain to adapt and reorganize essential behavioural and emotional functions [12].

The hippocampus plays an important role in learning and memory. In the streptozotocin-induced rat model, studies have described the loss of hippocampal neuroplasticity, a low proliferation rate in the dentate gyrus, poor neurogenesis, and a decrease in the number of hippocampal synapses [5, 20]. Our previous study has shown that the decline in hippocampal-related functions in diabetic individuals is not caused by the death of neurons in the hippocampus [20].

The loss of nerve fibres in the hippocampus is likely to be one of the critical reasons for cognitive decline. In the hippocampal neural circuit, impulses between neurons are mainly transmitted by nerve fibres, and changes in myelinated nerve fibres influence the conduction speed of nerve impulses, affecting the function of neural circuits.

Evidence from animal studies can help clarify the mechanism that causes cognitive decline in diabetic patients. STZ is a medication frequently used drug to cause diabetes in animal models [7, 20]. We used STZ injection intraperitoneally to establish a rat model of diabetes, then measured cognitive function after the diabetic rat models were fed a normal diet for 8 weeks. Current research has shown that in STZ-induced diabetic rats, the hippocampus is significantly affected which results in cognitive deficits.

Tang and Nyengard were the first to use stereology to perform a three-dimensional quantitative study of nerve fibres [17]. Stereology quantitative methods overcome the shortcomings of traditional quantitative methods, such as uniform random sampling in the entire area to be studied [8]. The result of this method is the total number amount of nerve fibres rather than the density [8]. Our research team reported for the first time that myelinated nerve fibres in the white matter, cortex, and hippocampus of the rat brain were significantly reduced with age by this method [22].

This study aimed to identify changes in the myelinated nerve fibres of the hippocampus associated with T1D-induced cognitive decline by stereology.

Therefore, in the present study, we examined the total volume of the hippocampus, the total length and volume of myelinated nerve fibres, and the total volume of myelin sheaths. Additionally, the distribution of the total length of myelinated nerve fibres under different diameters and myelin thicknesses was discussed.

This study is the first to detect changes in myelinated nerve fibres in T1D rats by stereological means to provide a basis for exploring the relationship between T1D-induced cognitive impairment and the ultrastructure of diabetic myelinated nerve fibres in the hippocampus.

MATERIALS AND METHODS

Experimental animals

A group of 4-month-old Sprague-Dawley (SD) rats ($n = 40$; 20 male rats and 20 female rats, North Sichuan Medical College, Nanchong, Sichuan, P.R. China) were housed at 23°C in a 60% humidity atmosphere under a 12 h-light-dark cycle, with free access to food and tap water. They were raised in the standard breeding cage of the SPF animal laboratory provided by Animal Research Institute of North Sichuan Medical College. An average of 3–5 animals per cage, and the animals adapted to the housing conditions for 3 days before the experiment. The indoor ventilation was at least 15 times per hour. The other housing conditions are keeping the ammonia concentration at less than 20 ppm, the relative humidity at 45–65%, the room temperature at 20–25°C, and keeping the room quiet. The animal care and treatment protocols were approved by the Animal Experimentation Ethics Committee of North Sichuan Medical College, Nanchong, Sichuan, P.R. China. All efforts were made to minimize animal suffering.

Induction of type 1 diabetes and experimental design

The rats were divided randomly into two groups, each group contained half males and half females. 20 rats (10 males and 10 females) were injected with streptozotocin (STZ) intraperitoneally (60 mg/kg body weight, S0130; Sigma, USA), which was dissolved with 0.01 M sodium citrate buffer (pH 4.3) as previously described [7, 20] and 20 control rats were injected with the sodium citrate buffer intraperitoneally. After one week, the blood glucose level was detected, and the rats with glucose levels > 16.7 mmol/L were confirmed to be successfully induced diabetes.

After 3 months of STZ injection, 4 rats died in the STZ group and 1 rat died in the control group. Among the rats successfully modelled in the STZ injection group, 12 rats (6 male rats and 6 female rats) were selected randomly as the type 1 diabetes model group (T1DM group). 12 healthy rats (half males and half females) without STZ injection were selected randomly as the control group. We found that STZ is currently the most widely used chemical inducer in animal models of diabetes, and it has a specific destructive effect on animal pancreatic islet β cells. The use of high-dose STZ causes animal islet cell necrosis and induces the development of T1D in animals. The STZ-induced model of T1D causes insulin deficiency, hyperglycaemia, polydipsia, and polyuria, much like T1D in humans. These symptoms of T1D are relatively easy to observe in rat models. The advantages of STZ-induced T1D models are that they are very similar to the process of human T1D, and T1D models are easy to establish, less expensive, and conducive to reproducibility [7, 20].

Morris water maze

After 3 months of STZ injection, the Morris water maze test was used to assess spatial memory [11, 21]. The set maze used a circular tank with a diameter of 120 cm and a height of 60 cm, which was filled with water ($23 \pm 2^\circ\text{C}$). The tank was divided into four quadrants. The escape platform (9 cm in diameter) was fixed in the pool 1–2 cm below the water surface. Each rat received four trials per day for four consecutive days. The starting point for each trial was chosen randomly. Each rat was put gently into the pool from any water entry point facing the pool wall. The swimming time to the platform (the escape latency) was recorded in each session. If the rats could not find the platform or did not get onto the platform within 180 s (the incubation period), they were guided onto the platform to rest for 15 s before the next test. The interval between the two tests was 30 minutes. The average value of four tests per day was taken as the result of that day. To determine if there were any visual defects displayed, the visible platform test was conducted.

Tissue processing

Five rats from each group were anesthetized using 4% chloral hydrate (10 ml/kg). They were perfused with 4% paraformaldehyde in 0.01 M phosphate-buffered saline (PBS, pH 7.4). The brain was

taken out and divided into two hemispheres along the median sagittal plane. The right or left hemisphere was sampled randomly. Each hemisphere was sliced into 1-mm-thick serial sections, and 12–15 sections were obtained from each cerebral hemisphere.

Estimation of the hippocampus volume

A transparent counting grid with an area of 0.1111 mm^2 associated with each point was placed at random on the caudal surface of each slab. The points hitting the hippocampus were counted (Fig. 1A), and the total hippocampal volume was calculated according to Cavalieri's principle [18, 22]:

$$V(\text{hip}) = t \times a(p) \times \sum P(\text{hip}) \times 2$$

where t was the section thickness (1 mm), $a(p)$ was the area associated with each grid point (0.1111 mm^2), and $\sum P(\text{hip})$ was the total number of grid points hitting the hippocampus per rat hemisphere.

Section preparation for transmission electron microscopy

Every third slab was sampled systematically from the first three slabs, with the first one being sampled randomly. A transparent counting grid was placed randomly on the caudal surface of the sampled slabs. The tissue blocks were obtained where the points in the sheet hit the hippocampus. The 1 mm^3 isometric tissue blocks were fixed in 2.5% glutaraldehyde at 4°C for 2 hours, washed with 0.1 M phosphate buffer (pH 7.4) three times, postfixed in 1% osmium tetroxide in 0.1 M phosphate buffer (pH 7.4) at 4°C for 2 hours, and dehydrated in a graded series of ethanol and acetone. With the sector embedded into 5 mm-diameter balls, the ball was placed in the horizontal plane and then embedded in the capsule according to the conventional transmission microscope embedding method. One section (70 nm) from each block was obtained using an ultramicrotome, and then the ultrathin sections were scanned in a Hitachi HT7700 TEM at 80 kV. Images were taken at a magnification of 6,000–15,000 \times . The photos of four fields of view at 6,000 \times magnification and eight fields of view at 15,000 \times magnification in each tissue block from each sample were equally spaced and randomly obtained [18, 22].

Unbiased stereological methods

Stereological counting of the total length of myelinated fibres in the hippocampus

An unbiased counting frame was superimposed onto the amplified image taken by the transmission

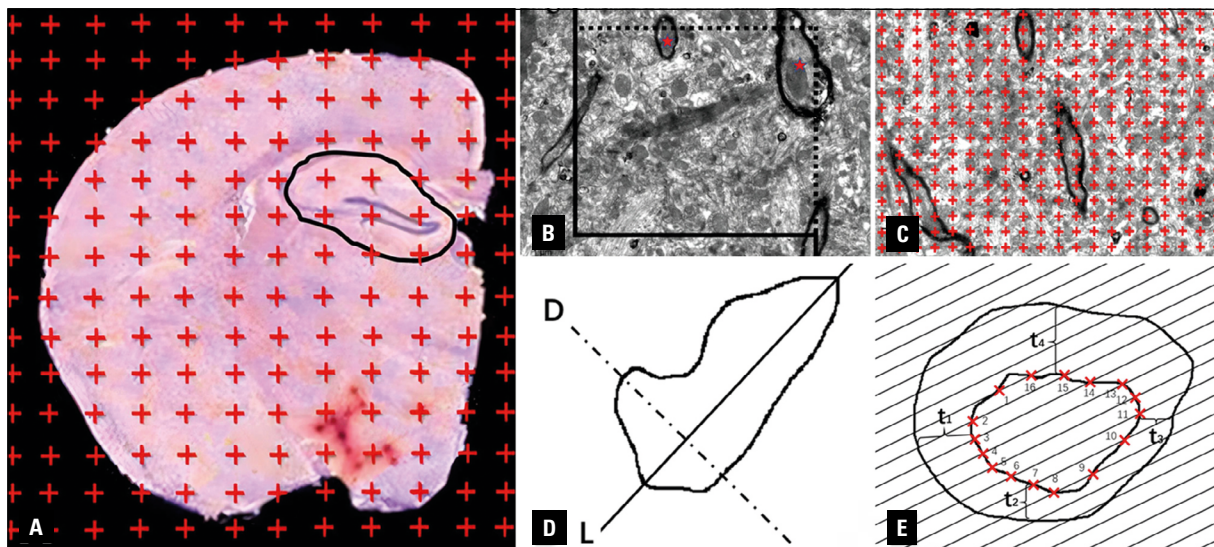


Figure 1. A. Figure showed a rat brain slice under anatomic microscope, and a point grid was superimposed on the slice at random. The points hitting the hippocampal formation were counted; B. The principle of unbiased counting frame. Myelinated fibres profiles inside the counting frame or touching the top and right lines (dotted line) were counted, and touching the left and bottom lines and the extensions of the right line and left line (solid line) were excluded from counting. Two profiles marked with ★ were counted in total. Scale bar = $1 \mu\text{m}$ ($\times 6000$); C. The points hitting the hippocampal formation, the myelinated fibres and the myelin sheaths were counted, respectively. Scale bar = $1 \mu\text{m}$ ($\times 6000$); D. The diameter of myelinated fibres sampled with the unbiased counting frame was estimated. First, the longest axis (L) of the myelinated nerve fibre section; E. The number of intersections, ΣI , between the inner boundary of the myelinated fibre profile and the equidistant test lines were counted (as shown, 16 intersections). The first number X was randomly chosen in the first 1/4-interval (as shown, I was 16, so the first position should be chosen from a random number between 1 and 4). Intersection 3 was randomly chosen as the first position. The second position was $X+1/4$ (intersection 7). The third position was $X+1/4 \times 2$ (intersection 11) and the fourth position was $X+1/4 \times 3$ (intersection 15). The mean thickness of myelin sheath equalled to the mean value of t_1 , t_2 , t_3 and t_4 .

electron microscope (Fig. 1B). Myelinated fibres intersecting with the inclusion line (dotted line) were counted, while fibres intersecting with the exclusion line (solid line) were excluded from the counting. The length density of myelinated fibres (LV) was calculated according to the formula [18, 22]:

$$LV = 2 \times \Sigma Q / \Sigma A$$

where ΣQ was the total number of myelinated fibres in unbiased counting frames and ΣA was the total area of the unbiased counting frames. The total length of myelinated fibre = length density \times hippocampus volume.

Stereological counting of the total volume of the myelin sheath in the hippocampus

A counting grid was superimposed onto the amplified image taken by the transmission electron microscope (Fig. 1C). The number of P(ms) on the myelin sheath and the number of hippocampus grid points within the entire photo (Ph) were counted. The volume density of the myelin sheath [V_v (ms)] was calculated according to the formula [18, 22]:

$$V_v \text{ (ms)} = \Sigma P(\text{ms}) / \Sigma \text{Ph}$$

Total volume of myelin sheath = V_v (ms) \times hippocampus volume

Calculation of the fibre diameter

The diameter of the nerve fibres was measured by an unbiased count (Fig. 1D). First, the longest axis of the myelinated nerve fibre section is determined. Then the longest transverse diameter perpendicular to the longest axis is the diameter of the myelinated nerve fibre section [8, 18, 22].

Average thickness of the myelin sheath in the hippocampus

The average thickness of the myelin sheath in the section was measured using the isometric test line (Fig. 1E). The number of intersections, ΣI , between the inner boundary of the myelinated fibre profile and the equidistant test lines were counted. The first number X was randomly chosen in the first 1/4-interval. Intersection 3 was randomly chosen as the first position. The second position was $X+1/4$. The third position was $X+1/4 \times 2$, and the fourth position was $X+1/4 \times 3$. The mean thickness of the

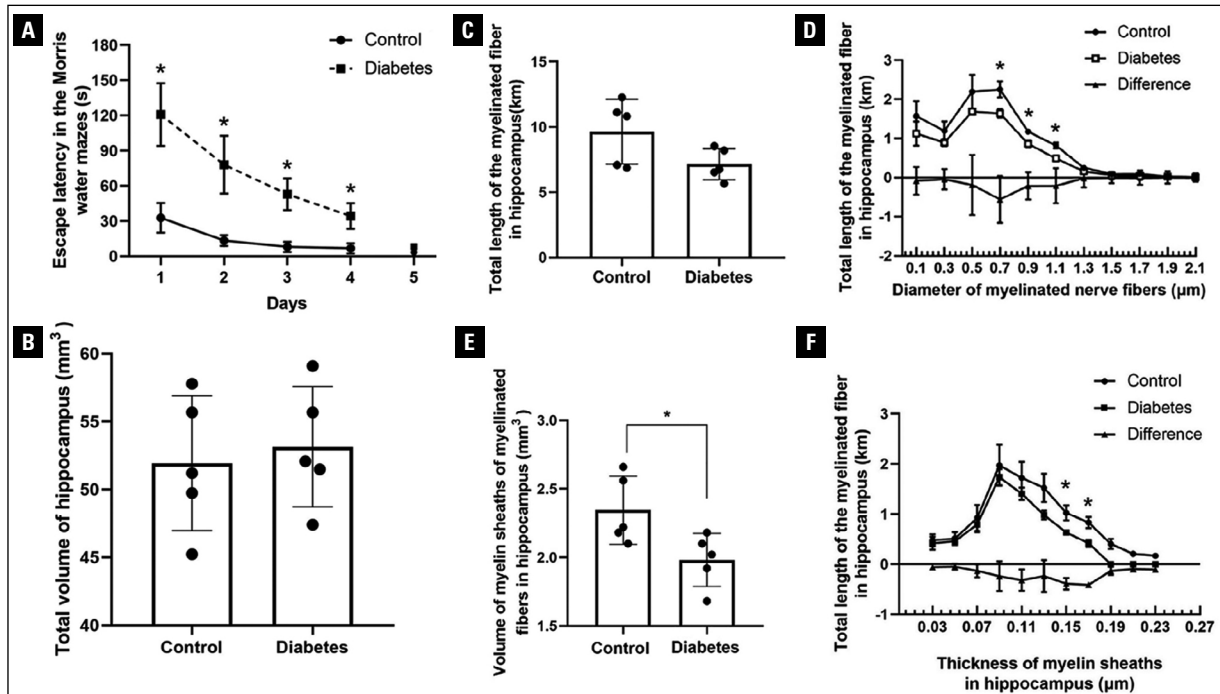


Figure 2. A. Comparison of the escape latency to the hidden platform between the control group and the diabetes group 3 months after STZ injection. Each point represented the mean \pm SD value of the trials. The rats were trained to find a hidden platform located in one quadrant of the water maze on Days 1–4 and to find a visible platform on Day 5 (* $p < 0.05$); B. Comparison of the total volume of the hippocampus between the control group and the diabetes group by stereological analysis; C. Comparison of the total length of myelinated fibres in the hippocampus between the control group and the diabetes group by stereological analysis; D. Absolute distributions of the total length of myelinated nerve fibres with different myelinated nerve fibre diameters in the hippocampus. The decrease in the total length of myelinated nerve fibres in the hippocampus of diabetic rats was mainly due to the increase in myelinated nerve fibres with diameters from 0.7 to 1.1 μm (* $p < 0.05$); E. Comparison of the total volume of the myelin sheath in the hippocampus between the control group and the diabetes group by stereological analysis. Compared with control rats, the average thickness of the myelin sheath in the hippocampus of diabetic rats was significantly reduced. (* $p < 0.05$); F. Absolute distributions of the total length of myelinated nerve fibres with different thicknesses of myelin sheaths in the hippocampus. When the thickness of the myelin sheath were from 0.15 to 0.17 μm , there were significant differences in myelinated nerve fibres between the diabetes group and the control group (* $p < 0.05$).

myelin sheath equalled the mean value of t1, t2, t3 and t4 [8].

Statistical analysis

SPSS 25 (IBM SPSS Inc., Chicago, IL, USA) was used for statistical analysis. Morris water maze data between the two groups from day 1 to 4 were analysed using repeated measures analysis of variance (ANOVA), and the data of day 5 was analysed with a one-way ANOVA. Unpaired, two-tailed Student's t-test was used to analyse whether the total length of myelinated fibres, the total volume of the myelin sheath and the average thickness of the myelin sheath were different between the control group and the diabetes group. A value of $p < 0.05$ was considered statistically significant [21, 22].

RESULTS

Behavioural testing

We selected all rats from both the remaining surviving control group and the diabetes group for Behavioural Testing. For the hidden platform on days 1–4, the escape latency of diabetic rats was significantly extended compared with that of the control group (* $p < 0.05$, Fig. 2A). For the visible platform on day 5, there was no significant difference in escape latency between the control group (3.3 ± 1.09 s) and the diabetes group (8.2 ± 4.82 s) ($p > 0.05$, Fig. 2A).

Changes in the total volume of the hippocampus

There was no significant difference in the total volume of the hippocampus between the control group (51.49 ± 6.26 mm³) and the diabetes group (53.25 ± 5.84 mm³) ($p > 0.05$) (Fig. 2B).

Changes in the total length and the distribution of the total length of myelinated nerve fibres with different myelinated nerve fibre diameters

As shown in Fig. 2C, when compared to the control group ($9.67 \text{ km} \pm 2.58$), the total length of myelinated nerve fibres in the hippocampus were decreased in the diabetic group ($6.76 \text{ km} \pm 1.09$), but the difference was not statistically significant ($p > 0.05$) (Fig. 2C).

When investigating the distribution of the total length of myelinated nerve fibres with different diameters in the control group and the diabetic group, there was a significant decrease with diameters of $0.7 \mu\text{m}$ ($*p = 0.035, < 0.05$), $0.9 \mu\text{m}$ ($*p = 0.018, < 0.05$) and $1.1 \mu\text{m}$ ($*p = 0.018, < 0.05$) (Fig. 2D).

Changes in total volume of myelin sheath and the distribution of the total myelinated fibres length with different thicknesses of myelin sheaths

The histogram in Figure 2E illustrates that, compared to the control group, the total volume of hippocampal myelin sheath of the diabetic group ($1.93 \text{ mm}^3 \pm 0.25$) was significantly different ($2.33 \text{ mm}^3 \pm 0.23$) ($*p = 0.028, < 0.05$) (Fig. 2E).

Moreover, as shown in Fig. 2F, the distribution of the total myelinated fibres length with different myelin sheath thicknesses. We found that, compared to the control group, the significant decrease in the myelinated fibre length in the diabetic group was mainly due to the decreases in myelinated fibres with myelin sheath thicknesses from 0.15 to $0.17 \mu\text{m}$. When the myelin sheath thicknesses were $0.15 \mu\text{m}$ ($*p = 0.038, < 0.05$) and $0.17 \mu\text{m}$ ($*p = 0.012, < 0.05$) (Fig. 2F), the total length of myelinated nerve fibres was statistically significant between the control group and the diabetes group.

DISCUSSION

In humans, diabetes is associated with moderate impairment of cognitive function, and patients are at high risk of affective disorders, dementia, and Alzheimer's disease [10, 13]. In the present study, the diabetic rats showed prolonged escape latency compared to the normal rats, suggesting that the diabetic rats exhibited spatial learning and memory dysfunction, which was consistent with the results of previous similar studies [5, 20, 21]. Frøkjær et al. found that patients with long-term T1D did not show any significant structural changes in grey matter and white matter volume, cortical thickness, or morpho-

logical changes [2]. However, cortical thinning was observed in sensory-related areas, which is related to the presence of peripheral neuropathy [2]. In addition, Kodl et al. found that fibrous tissue was reduced in T1D, indicating that posterior coronal radiation and optic radiation demyelination are related to neurocognitive performance and the course of diabetes [6]. The hippocampus plays a vital role in human learning and memory and is known to be susceptible to stress and disease. A large amount of literature shows that humans rely on the hippocampus for specific types of nonspatial and spatial memories (called declarative and relational) [9]. When humans encode or retrieve these same types of spatial and nonspatial memories, the hippocampus is activated [9]. An increasing number of preclinical studies provide sufficient evidence that diabetes negatively affects the morphological integrity of the hippocampus, and that the reduction in hippocampal neurogenesis is consistent with other forms of neuroplasticity defects, which may lead to the development of diabetic comorbidities and emotional symptoms [16]. In our previous research, diabetic-induced cognitive dysfunction may be related to the degeneration of synaptic number [20] and hippocampal capillary [21]. Our previous findings indicated that in the early stage of diabetic cognitive dysfunction, when compared to control rats, the total neuron number in the hippocampus changed insignificantly; however, the total number of spinophilin/neurabin-positive boutons significantly decreased by 69.6% [20]. What kind of role do the nerve fibres between neurons and synapses play? Little is known about the association between myelinated fibre changes and the central nervous system in type 1 diabetes.

The highly ordered communication system in the brain requires the complete structure and normal function of myelinated nerve fibres. Myelinated fibres have evolved to enable fast and efficient transduction of electrical signals in the nervous system. To act as an electrical insulator, the myelin sheath is formed as a multilamellar membrane structure by spiral wrapping and subsequent compaction of the oligodendroglial plasma membrane around CNS axons. Bak et al. reported that neurotransmitter metabolism has a key role in maintaining normal cognitive function, especially the glutamate/GABA-glutamine (Glu/GABA-Gln) cycle [1]. In the Glu/GABA-Gln cycle, although glutamine is an excitatory neurotransmitter, it first directly transforms into the inhibitory neuro-

transmitter glutamate, and then indirectly transforms into the inhibitory neurotransmitter GABA. Gao et al. demonstrated that diabetes-induced cognitive decline could be attributed to a disrupted Glu/GABA-Gln cycle [3]. Zheng et al. recently reported that the gut microbiota from schizophrenic patients altered the Glu/GABA-Gln cycle in the hippocampus, causing schizophrenic-relevant behaviours in mice, which may provide indirect evidence [23]. This hypothesis still needs to be validated further.

Unbiased stereological quantitative methods overcome the shortcomings of traditional quantitative methods, such as uniform random sampling in the entire area to be studied [8, 22]. The result of this method is the total amount of nerve fibres instead of their density. According to this method, this study reported the changes in myelinated nerve fibres in the hippocampus of T1D rats for the first time.

In the present results, there was no difference in total hippocampal volume between diabetic and control rats. It suggested that the direct point of change was not simply due to the hippocampus itself but the myelinated nerve fibres in the hippocampus.

It is generally accepted that changes in myelinated nerve fibres are crucial to the formation of the hippocampus as a basic component of the hippocampus [14]. In our present findings, when compared to control rats, we observed a significantly decreased total myelin sheath volume in the hippocampus of diabetic rats. Therefore, we speculated that the reduced myelin sheath of myelinated nerve fibres could be responsible for diabetes-induced cognitive dysfunction. In particular, we found that, in the hippocampus of the diabetes group, the total myelinated fibre length was significantly decreased, especially with diameters from 0.7 to 1.1 μm , which may indicate that smaller fibres are more vulnerable to damage in diabetes.

At the same time, we also measured the changes in the total length of myelinated nerve fibres with different myelin sheath thicknesses. We found a significant decrease in total length of fibres with the myelin sheath thickness from 0.15 to 0.17 μm . The results showed that myelinated nerve fibres with smaller diameters and/or thinner myelin sheaths were more vulnerable and susceptible to diabetes-related cognitive dysfunction. However, whether a relationship between the myelinated nerve fibres of the hippocampus and T1D-induced cognitive impairment exists still needs to be further explored.

In conclusion, the results of this study provide insights into the mechanistic correlation between hippocampal myelinated fibres and STZ-induced diabetic rats. We conclude that there are likely to be multiple factors contributing to cognitive decline in T1D individuals, and changes in the myelin sheath of nerve fibres may represent one of them. Subsequently, our future research will further explore the macrostructural and molecular mechanisms of the changes in the myelinated nerve fibres of the hippocampus in T1D.

ARTICLE INFORMATION AND DECLARATIONS

Acknowledgments

This research was supported by National Natural Science Foundation of China (Grant Number: 81400806); Project of The Health Planning Committee of Sichuan (Grant Number: 17PJ081); Project of The Health Planning Committee of Sichuan (Grant Number: 20PJ181).

Conflict of interest: None declared.

REFERENCES

1. Bak LK, Schousboe A, Waagepetersen HS. The glutamate/GABA-glutamine cycle: aspects of transport, neurotransmitter homeostasis and ammonia transfer. *J Neurochem*. 2006; 98(3): 641–653, doi: [10.1111/j.1471-4159.2006.03913.x](https://doi.org/10.1111/j.1471-4159.2006.03913.x), indexed in Pubmed: [16787421](https://pubmed.ncbi.nlm.nih.gov/16787421/).
2. Frøkjær JB, Brock C, Søfteland E, et al. Macrostructural brain changes in patients with longstanding type 1 diabetes mellitus - a cortical thickness analysis study. *Exp Clin Endocrinol Diabetes*. 2013; 121(6): 354–360, doi: [10.1055/s-0033-1345120](https://doi.org/10.1055/s-0033-1345120), indexed in Pubmed: [23757052](https://pubmed.ncbi.nlm.nih.gov/23757052/).
3. Gao H, Jiang Q, Ji H, et al. Type 1 diabetes induces cognitive dysfunction in rats associated with alterations of the gut microbiome and metabolomes in serum and hippocampus. *Biochim Biophys Acta Mol Basis Dis*. 2019; 1865(12): 165541, doi: [10.1016/j.bbadis.2019.165541](https://doi.org/10.1016/j.bbadis.2019.165541), indexed in Pubmed: [31472216](https://pubmed.ncbi.nlm.nih.gov/31472216/).
4. Guan Yi, Ebrahimzadeh SA, Cheng CH, et al. Alzheimer's Disease Neuroimaging Initiative. Association of Diabetes and Hypertension With Brain Structural Integrity and Cognition in the Boston Puerto Rican Health Study Cohort. *Neurology*. 2022; 98(15): e1534–e1544, doi: [10.1212/WNL.000000000000200120](https://doi.org/10.1212/WNL.000000000000200120), indexed in Pubmed: [35354581](https://pubmed.ncbi.nlm.nih.gov/35354581/).
5. Ho N, Sommers MS, Lucki I. Effects of diabetes on hippocampal neurogenesis: links to cognition and depression. *Neurosci Biobehav Rev*. 2013; 37(8): 1346–1362, doi: [10.1016/j.neubiorev.2013.03.010](https://doi.org/10.1016/j.neubiorev.2013.03.010), indexed in Pubmed: [23680701](https://pubmed.ncbi.nlm.nih.gov/23680701/).
6. Kodl CT, Franc DT, Rao JP, et al. Diffusion tensor imaging identifies deficits in white matter microstructure in subjects with type 1 diabetes that correlate with reduced neu-

- rocognitive function. *Diabetes*. 2008; 57(11): 3083–3089, doi: [10.2337/db08-0724](https://doi.org/10.2337/db08-0724), indexed in Pubmed: [18694971](https://pubmed.ncbi.nlm.nih.gov/18694971/).
7. Koellisch U, Laustsen C, Nørting TS, et al. Investigation of metabolic changes in STZ-induced diabetic rats with hyperpolarized [1-¹³C]acetate. *Physiol Rep*. 2015; 3(8), doi: [10.14814/phy2.12474](https://doi.org/10.14814/phy2.12474), indexed in Pubmed: [26272734](https://pubmed.ncbi.nlm.nih.gov/26272734/).
 8. Li C, Yang S, Chen L, et al. Stereological methods for estimating the myelin sheaths of the myelinated fibers in white matter. *Anat Rec (Hoboken)*. 2009; 292(10): 1648–1655, doi: [10.1002/ar.20959](https://doi.org/10.1002/ar.20959), indexed in Pubmed: [19718718](https://pubmed.ncbi.nlm.nih.gov/19718718/).
 9. Lisman J, Buzsáki G, Eichenbaum H, et al. Viewpoints: how the hippocampus contributes to memory, navigation and cognition. *Nat Neurosci*. 2017; 20(11): 1434–1447, doi: [10.1038/nn.4661](https://doi.org/10.1038/nn.4661), indexed in Pubmed: [29073641](https://pubmed.ncbi.nlm.nih.gov/29073641/).
 10. Moheet A, Mangia S, Seaquist ER. Impact of diabetes on cognitive function and brain structure. *Ann N Y Acad Sci*. 2015; 1353: 60–71, doi: [10.1111/nyas.12807](https://doi.org/10.1111/nyas.12807), indexed in Pubmed: [26132277](https://pubmed.ncbi.nlm.nih.gov/26132277/).
 11. Morris RG, Garrud P, Rawlins JN, et al. Place navigation impaired in rats with hippocampal lesions. *Nature*. 1982; 297(5868): 681–683, doi: [10.1038/297681a0](https://doi.org/10.1038/297681a0), indexed in Pubmed: [7088155](https://pubmed.ncbi.nlm.nih.gov/7088155/).
 12. Morton H, Kshirsagar S, Orlov E, et al. Defective mitophagy and synaptic degeneration in Alzheimer's disease: Focus on aging, mitochondria and synapse. *Free Radic Biol Med*. 2021; 172: 652–667, doi: [10.1016/j.freeradbiomed.2021.07.013](https://doi.org/10.1016/j.freeradbiomed.2021.07.013), indexed in Pubmed: [34246776](https://pubmed.ncbi.nlm.nih.gov/34246776/).
 13. Northam EA, Rankins D, Cameron FJ. Therapy insight: the impact of type 1 diabetes on brain development and function. *Nat Clin Pract Neurol*. 2006; 2(2): 78–86, doi: [10.1038/ncpneuro0097](https://doi.org/10.1038/ncpneuro0097), indexed in Pubmed: [16932529](https://pubmed.ncbi.nlm.nih.gov/16932529/).
 14. Qiu X, Huang CX, Lu W, et al. Effects of a 4 month enriched environment on the hippocampus and the myelinated fibers in the hippocampus of middle-aged rats. *Brain Res*. 2012; 1465: 26–33, doi: [10.1016/j.brainres.2012.05.025](https://doi.org/10.1016/j.brainres.2012.05.025), indexed in Pubmed: [22627162](https://pubmed.ncbi.nlm.nih.gov/22627162/).
 15. Teh K, Wilkinson ID, Heiberg-Gibbons F, et al. Central nervous system involvement in diabetic neuropathy. *Curr Diab Rep*. 2011; 11(4): 310–322, doi: [10.1007/s11892-011-0205-z](https://doi.org/10.1007/s11892-011-0205-z), indexed in Pubmed: [21667355](https://pubmed.ncbi.nlm.nih.gov/21667355/).
 16. Stranahan AM. Models and mechanisms for hippocampal dysfunction in obesity and diabetes. *Neuroscience*. 2015; 309: 125–139, doi: [10.1016/j.neuroscience.2015.04.045](https://doi.org/10.1016/j.neuroscience.2015.04.045), indexed in Pubmed: [25934036](https://pubmed.ncbi.nlm.nih.gov/25934036/).
 17. Tang Y, Nyengaard JR. A stereological method for estimating the total length and size of myelin fibers in human brain white matter. *J Neurosci Methods*. 1997; 73(2): 193–200, doi: [10.1016/s0165-0270\(97\)02228-0](https://doi.org/10.1016/s0165-0270(97)02228-0), indexed in Pubmed: [9196291](https://pubmed.ncbi.nlm.nih.gov/9196291/).
 18. Tang Y, Pakkenberg B, Nyengaard JR. Myelinated nerve fibres in the subcortical white matter of cerebral hemispheres are preserved in alcoholic subjects. *Brain Res*. 2004; 1029(2): 162–167, doi: [10.1016/j.brainres.2004.09.035](https://doi.org/10.1016/j.brainres.2004.09.035), indexed in Pubmed: [15542070](https://pubmed.ncbi.nlm.nih.gov/15542070/).
 19. Xie K, Perna L, Schöttker B, et al. Type 2 diabetes mellitus and cognitive decline in older adults in Germany — results from a population-based cohort. *BMC Geriatr*. 2022; 22(1): 455, doi: [10.1186/s12877-022-03151-y](https://doi.org/10.1186/s12877-022-03151-y), indexed in Pubmed: [35619073](https://pubmed.ncbi.nlm.nih.gov/35619073/).
 20. Zhao F, Li J, Mo L, et al. Changes in neurons and synapses in hippocampus of streptozotocin-induced type 1 diabetes rats: a stereological investigation. *Anat Rec (Hoboken)*. 2016; 299(9): 1174–1183, doi: [10.1002/ar.23344](https://doi.org/10.1002/ar.23344), indexed in Pubmed: [27064698](https://pubmed.ncbi.nlm.nih.gov/27064698/).
 21. Zhao Y, Liu J, Li J, et al. Changes in hippocampal capillaries in transgenic type 2 diabetic mice: a stereological investigation. *Anat Rec (Hoboken)*. 2021; 304(5): 1071–1083, doi: [10.1002/ar.24525](https://doi.org/10.1002/ar.24525), indexed in Pubmed: [33015956](https://pubmed.ncbi.nlm.nih.gov/33015956/).
 22. Zhao YY, Shi XY, Qiu X, et al. Enriched environment increases the myelinated nerve fibers of aged rat corpus callosum. *Anat Rec (Hoboken)*. 2012; 295(6): 999–1005, doi: [10.1002/ar.22446](https://doi.org/10.1002/ar.22446), indexed in Pubmed: [22431229](https://pubmed.ncbi.nlm.nih.gov/22431229/).
 23. Zheng H, Lin Q, Wang D, et al. NMR-based metabolomics reveals brain region-specific metabolic alterations in streptozotocin-induced diabetic rats with cognitive dysfunction. *Metab Brain Dis*. 2017; 32(2): 585–593, doi: [10.1007/s11011-016-9949-0](https://doi.org/10.1007/s11011-016-9949-0), indexed in Pubmed: [28070703](https://pubmed.ncbi.nlm.nih.gov/28070703/).